Article

Reepithelization of damaged cornea in the presence of multi-walled carbon nanotubes

Viktoria Baksa, Alexandra Kiss, Melinda Turani, Laszlo Talas, Richard Kovasznai Olah, Gyula Pinczes, Zsuzsa M. Szigeti, Gabor Szeman-Nagy§ and Gaspar Banfalvi§*

* Gabor Szeman-Nagy and Gaspar Banfalvi contributed euqually to the MS; Department of Molecular Biotechnology and Microbiology; University of Debrecen, 1 Egyetem Square, Debrecen 4010, Hungary

* Correspondence: Email: banfalvi.gaspar@science.unideb.hu; Tel.: +36-52-512-900 (ext. 62319); Fax: +36-52-512-925

Abstract: Increased number of airborne particles upon accidents may cause corneal damages. The purpose of this study was to determine the smallest dose of multi-walled carbon nanotubes (MWCNT) that would interfere with corneal re-epithelization., The effect of multi-walled carbon nanotubes (MWCNT) in cornea damages was investigated *in vitro* and *in vivo.* Murine *in vivo* experiments were performed with intact, non-functionalized MWCNTs to confirm the validity of *in vitro* tests. The MWCNTs 10-30 μm in length and 10 -30 nm outer diameter at low concentration (5 μg/ml) did not interfere with the wound healing of the damaged limbal cell monolayer. Higher than 50 μg/ml concentrations: a) generated MWCNT aggregates, b) restrained the movement and prolonged the time of wound healing, c) increased the amplitudes of the oscillations of the cells, and d) resulted in scar formation affecting both corneal function and refraction. MWCNTs are prone to form aggregates and prevent to slow down the regeneration of corneal wounds. Results confirmed that human limbal cell regrowth mimicked by the *in vitro* scratch model was slowed down by aggregates of MWCNTs. The size of the aggregates was proportional to the concentration of MWCNTs applied. *In vivo* results performed in mice confirmed *in vitro* tests and suggested that time-lapse microscopy is a useful means to follow the regeneration of cellular damages. These deposits have to be removed or at least minimized before corneal scar formation would take place. Chromatin condensation was completed and metaphase chromosomes were seen at higher MWCNT concentration by time-lapse microscopy proving that their aggregates did not affect the viability of limbal cells.

Keywords: Cytotoxicity; Limbal stem cells; Corneal healing; Time-lapse imaging; Mimicking reepithelization; Toxicity of MWCNT aggregates

1. Introduction

The limbal ophthalmic scratch assay is an easy, low-cost and well-developed method to measure cell migration *in vitro*. The basic steps involve creating a "scratch" in a cell monolayer, capturing the images at the beginning and at regular intervals during cell migration to close the scratch, and comparing the images to quantify the migration rate of the cells. Compared to other methods, the in vitro scratch assay is particularly suitable for studies on the effects of cell-matrix and cell-cell interactions on cell migration, during wound healing in vivo and are compatible with imaging of live cells during migration to monitor intracellular events if desired [1]. We have used originally the in vitro scratch model: a) to see how antibiotics delay in vitro human limbal stem cell regrowth [2], b) the regeneration of limbal stem cells in the presence of silver and gold nanoparticles [3]. In

this paper we have extended the in vitro scratch to an in vivo mouse model and investigated how multi-walled carbon nanotubes (MWCNT) interfere with corneal re-epithelization.

The ocular system involves the visual system of the eye: cornea, lens, fuids (Fig. 1). The function of the ocular system is to transduce light into visual signals by means of epithelial cells (primarily limbal cells), keratocytes, fibroblasts, and trabecular meshwork cells. Ultrafine particles also known as nanoparticles between 1 and 100 nm in size disturb the function of the visual system. Exponentially growing research efforts contributed to the potential human health hazard posed by nanoparticles, yet understanding regarding their genotoxicity remained limited. Carbon nanotubes are organized graphene sheets consisting of one or more layers [4]. The size of nanotubes used in this study was 10-30 nanometer outer diameter and 10-30 μm length corresponding to the size of often occurring man-made pollutants. Such nanoparticles are present in the combustion products of fuels, which makes contact with them unavoidable. The biological impact of nanoparticles is poorly understood, but likely to be unique and characteristic to the type of nanoparticle. The best-studied fullerene carbon nanotubes include single-walled carbon nanotubes (SWCNTs) and multi-walled carbon nanotubes (MWCNTs) [5]. SWCNTs and MWCNTs are currently under intensive investigation. SWCNTs are promising candidates for cancer chemotherapy delivery, especially when functionalized with anticancer drugs that induce apoptosis (e.g. combretastatin A4, CA4). Experimental data suggest that SWCNT-CA4 has anticancer activity superior to that of free CA4 [6]. However, functionalization of SWCNTs by binding to proteins may significantly impact the cytotoxicity of nanotubes. The binding of BSA to SWCNTs reduced cytotoxicity and the degraded nanotubes induced less cytotoxicity than non-degraded nanotubes [7].

Multi-walled carbon nanotubes are known to cause potentially hazardous effects on intracellular and extracellular pathways. Bronchial epithelial cells and mesothelial cells are crucial targets for the safety assessment of inhalation of carbon nanotubes, which resemble asbestos particles in shape [8]. When the cytotoxicity of two different types of MWCNTs in A549 lung epithelial cells and HepG2 hepatocytes was investigated, heat-treated MWCNTs showed significantly stronger adverse effects compared to the non-treated MWCNTs. Moreover, heat-treated MWCNTs induced a dose-dependent cell cycle arrest in A549 cells and leading to a decrease in surface defects [9]. The topical application of low doses of MWCNTs in mice induced keratinocyte cytotoxicity and exacerbation of allergic skin conditions in a carboxylation dependent manner. However, neither functionalized (doped) MWCNTs increased the level of in vitro reactive oxygen species in HaCaT keratinocyte cell line [10]. Formononetin (FMN), and functionalized multi-walled carbon nanotube composites (MWCNT-COOH, MWCNT-FMN) were used to induce apoptosis via reactive oxygen species (ROS) production in murine fibroblast 3T3 and HeLa cells. The in vitro cytotoxicity assay was performed using water-soluble tetrazolium assay and demonstrated that FMN, MWCNT-COOH, and MWCNT-FMN had no significant effects on the proliferation and viability of mouse fibroblast 3T3 cells while the cell growth inhibition of the three samples showed concentration-dependence for HeLa cells [11].

Pulmonary exposure to MWCNTs gave contradictory results. MWCNTs could generate lung inflammation, fibrosis, and cancer among those exposed to it. However, there are currently no effective biomarkers for detecting lung fibrosis or predicting the risk of lung cancer resulting from MWCNT exposure [12]. MWCNTs have been shown to induce lung fibrosis in animal models [13]. To the contrary, gene-specific DNA methylation status was tested upon treatment of human lung cells with SWCNTs, MWCNTs + asbestos and asbestos alone. MWCNT-exposed cells showed significant global DNA hypomethylation of cytosine and global RNA hypomethylation of adenosine. SWCNT, MWCNT, and amosite (asbestos) exposure decreased the DNA methylation pattern [14].The applications of multi-walled nanocarbon tubes (MWCNTs) in the composite-material industry raised questions about their short and long-term health effects. Although studies of rats upon inhalation of MWCNTs produced no systemic toxicity [15], conclusive results were not

obtained. MWCNTs toxicity tests need comparable and standardized conditions concerning cell line, animal species, exposure conditions [16]. as well as size, shape, purity, and functionalization of nanotubes [17]. The diameter was found to be inversely related to the bioactivity of MWCNTs preparations, and carboxyl- or amino-functionalization could be at least in part, attributable to the greater tendency of functionalized MWCNTs to form large agglomerates in protein-rich biological fluids [18]. In spite of efforts, the elucidation of toxicity determinants of multi-walled carbon nanotubes (MWCNTs) remained limited. The research of nanoparticles in the automobile industry has focused on the release of nanoparticles by vehicle exhaust, brakes, catalytic converter and at road-tire abrasion processes [19] but not on the MWCNTs generated in fires or car exhaust pipes. It was found that 1.5 wt% of MWCNTs enhanced significantly the mechanical properties of automobile bumpers. Less attention was paid to those MWCNTs and their aggregates that were released by accidents and aeroplane crashes [20].

The risk of eye injuries in car accidents in the US has been confirmed among males, 15 to 19 years old [21]. Corneal diseases, applications of nanotubes in drug-delivery and corneal disease management deserve special attention [22]. Nevertheless, the effects on corneal injuries contaminated with MWCNTs and aggregates of MWCNTs are poorly characterized.

Limbal epithelial culture is used to further our understanding of limbal stem-cell biology, for the culture expansion of limbal stem cells for transplantation purposes in patients with limbal stem-cell deficiency [23] or damage of the epithelial surface of eyes described in this paper. HuLi cells were regarded as stem cells [24,25. Recent studies show that stem cell-derived extracellular vesicles (EVs) play a relevant role in stem cell-induced regeneration by reprogramming injured cells and inducing proregenerative pathways. EVs derived from mesenchymal stem cells are able to promote regeneration of damaged human corneal epithelial cells [26].

We have established a cell line from the human limbal area to study the in vitro cell growth and response to the toxic effects of antibiotics used in ophthalmology [3]. The cytotoxic effects were evaluated by monitoring the proliferation, measuring the cellular motility and following chromatin changes in various cell lines upon MWCNT treatment. Measurements applied long-term scanning microscopy and a perfusion platform that replaced the medium with test solutions, bypassed physical contact with the cell culture during experiments, and provided uninterrupted high time-resolution time-lapse photomicrography for an extended period of time. Genotoxicity specific chromatin changes characteristic to toxic effects were distinguished in human skin keratinocytes (HaCaT), human limbal cells (HuLi), colorectal adenocarcinoma ($CaCO_2$), murine squamous carcinoma (SCC) and Indian muntjac (IM) cell lines [

2. Materials and Methods

2.1. Materials

DABCO (1,4-diazobicyclo-(2,2,2)-octane), Penicillin-Streptomycin-Neomycin antibiotics (PSN-375963) were from Sigma-Aldrich, Budapest, Hungary. 2,6- diamino-2-phenylindole (DAPI) was the product of Braunschweig Chemie (Braunschweig, Germany). Dextran T-150 was purchased from Pharmacia-Biochemicals (Uppsala, Sweden). Colcemid (N-methyl-N-deacetyl-colchicine) was the product of Boehringer (Mannheim, Germany). To eliminate bacterial contamination sterile-filtered PSN antibiotics were used. Penicillin-Streptomycin-Neomycin antibiotics (PSN-375963) were from Sigma-Aldrich, Budapest, Hungary.

Dulbecco's Modified Eagle's Medium Nutrient Mixture (DMEM-HAM'S F12) (Sigma-Aldrich, Budapest, Hungary) was supplemented with 2 mM L-glutamine, 23 mM sodium bicarbonate, 10% Fetal Bovine Serum (FBS) (Hyclon, Logan, UT) and 1% PSN (Sigma-Aldrich, Budapest, Hungary). Multi-walled carbon nanotubes of 10-30 nm outer

diameter (OD) and 10-30 μm length were provided by the producer Sun Innovations Inc (Fremont, CA, USA).

Nanotubes were suspended in sterile PBS, ultrasound-sonicated in an Ultrashall Reiniger Emmi 4 (EMAG AG, Mörfelden-Walldorf, Germany) ultrasonic homogenizer for 30 sec at room temperature. Nanotubes were homogenized again individually right before using the tube containing MWCNT in a Vortex shaker at 1000 rpm for a 2x5 sec to reduce the formation of macroaggregates.

MWCNTs here refer to those multi-walled carbon nanotubes (MWCNTs) that were used to treat limbal cell cultures at 5, 50, 100 and 500μg/ml concentrations and to follow the healing process of scratched murine eyes *in vivo* at 500μg/ml in sterile saline solution.

2.2. Methods

Kang et al. demonstrated that the uptake of sub-μm MWCNTs internalized easier through an energy-independent pathway [27]. [29]. Multi-walled carbon nanotubes 0.5–2 μm in length, 10–30 nm in our diameter were excluded from the interior of the cell [28.] The poor dispersion in saline media resulted in the aggregation of MWCNTand suggested that they do not enter the much smaller cells.

2.2.1. Establishment of human limbal cell line

The corneoscleral limbal rim originated from an enucleated eye of a 56 years old female patient's cadaver. The human limbal cell line used in the present investigation was described earlier [29]. .

2.2.2. Trypan blue test

The trypan blue exclusion assay is a standard, inexpensive and fast method that needs only a small fraction of the cell population to distinguish viable cells from dead cells by light microscopy. The trypan blue inclusion does not differentiate between apoptosis and necrosis. Although apoptosis causes shrinkage and necrotic enlargement of dying cells, this is not necessarily seen by the trypan blue test, as the process of cell death may take place within minutes or last for days. The use of trypan blue is limited by the tiresome counting of each individual sample, by its subjective evaluation, by staining only necrotic or late apoptotic cells. The following simple protocol was used to determine cell viability by the trypan blue test [30]:

1. Add 0.1 ml of 0.5% trypan blue in isotonic salt solution (saline, PBS) to 0.1 ml cells in the same solution.

2. Load the stained cells immediately on a hemacytometer, place the hemacytometer under the light microscope at low magnification (dilute if necessary with PBS).

3. Count the number of blue (dead) and white (live) stained cells, the sum of which gives the total cell number. Cell viability is calculated as the number of viable cells divided by the total number of cells within the grids of the hemacytometer.Trypan blue does not stain intact cells. Occasionally it may be observed that immediately after the addition of trypan blue permeability changes cause the slow infiltration of the stain and cells become first light blue then dark blue. Trypan blue stains dead (apoptotic and necrotic) cells dark blue.

2.2.3. Animal care

Inbred BALB/c mice were obtained from Charles River Animal Lab Kft, Budapest, Hungary. Both sexes of mice (10-12 weeks old, 20 ± 3 g of weight) were used in experiments. Animals have kept in PI plastic cages (425/135/120 mm, 573.75 cm^2) with mesh covers according to the guidelines of 2010/ 63/EU. Animals were fed with pelleted mouse chow (Purina, LabDiet, St. Louis, MO, USA) and tap water *ad libitum*. Automated room illumination of 12 h light and 12 h dark cycles, and room temperatures between 22–25 °C

Preprints (www.preprints.org) | NOT PEER-REVIEWED | Posted: 26 April 2023 doi:10.20944/preprints202304.0986.v1

were maintained. Animal experiments were carried out in our Experimental Animal Facility (reg. num.: III/3.-KÁT/2015) under the supervision of the Animal Care Committee, University of Debrecen. The experimental protocols were approved by the Animal Care Committee (Licence number: 2/2014 DEMAB). Animal experiments and care conformed to the general guidelines of the protection of the European Community (86/609/EEC) and special guidelines of BSL2 (200/54/EC 16/1). Human protection included respiratory protective equipment by observing the Health Protection Agency facemask guidelines and using the standard FFP2 equivalent to the N95 HEPA filter [30].

2.2.4. In vitro and in vivo models mimicking corneal epithelial growth

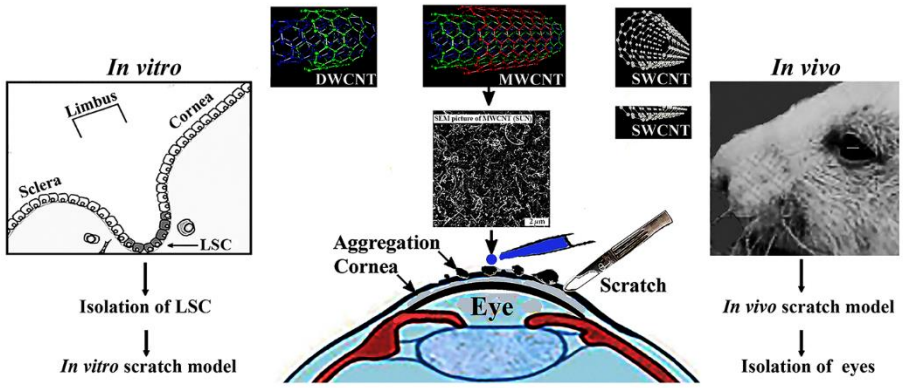

Figure 1. The *in vitro* scratch model (to the left) and the *in vivo* scratch wound model (to the right) is shematically depicted. The in vitro model mimics cell behaviour during wound healing in a confluent cell layer [3]. In the in vivo model the smudging of the damaged cornea was avoided during scratching by a sharply cut metal tip of a sterile hypodermic needle (average diameter 0.8-.0.9 mm). Modified with permission [3]. Increased number of airborne particles upon accidents may cause corneal damages. The effect of multiwalled carbon nanotubes (MWCNT) (10-30 μm in length and 10-30 nm in diameter) was investigated on confluent monolayer culture of *in vitro* and *in vivo* on corneal wound healing. MWCNTs are prone to form aggregates and prevent to slow down limbal cells. The regeneration of corneal wounds caused by the scratch in the eyes of mice is shown at the right side of Fig. 1. The experiment was designed to confirm that human limbal cell regrowth mimicked by the *in vitro* scratch model of corneal trauma was slowed down by aggregates of MWCNTs. The size of the aggregates was proportional to the concentration of MWCNTs applied. *In vivo* results performed in mice confirmed *in vitro* tests and suggested that time-lapse microscopy is a useful means to follow the regeneration of cellular damages. These deposits have to be removed or at least minimized before corneal scar formation would take place.

2.2.5. Treatment of limbal cell cultures with nanotubes

The stock mixture of MWCNTs carefully dispersed in PBS was diluted with 10% PBS containing growth medium (F12-Ham + 10% FBS + 1% PSN). The size measurement of aggregated MWCNTs was performed as described in the Methods using the ImageJ software program. The size distribution of aggregated nanotubes at 5, 50 and 100 μg/ml concentrations in the growth medium showed that at low concentration (5 μg/ml) the tendency of aggregation was lower, than at medium (50 μg/ml) and higher (100 μg/ml) nanoparticle concentrations. This tendency is accounted for by the strong non-polar character of nanotubes and strengthened by the presence of the growth medium primarily by the relatively high (10%) concentration of FBS. At the highest concentration (500 μg/ml) of MWCNTs, the size of their aggregates could not be measured.The size of the macroaggregates was selected by the progressive washing and trypsinization. At the highest (500 μg/ml) MWCNT concentration largest size reduction of macroaggregates was observed after the removal of the supernatant probably because the largest aggregates were floating and did not bind to the growth surface. These experiments were carried out in cell cultures at 20% confluency grown for 72 h in the presence of different

concentrations of MWCNT corresponding to 5, 50, 100 or 500 μg/ml. The surface area of macroaggregates at these concentrations and after treatments (trypsin and osmotic shock) were given in μm².

2.2.6. Time-lapse scanning (TLS) microscopy

Diodes emitting light at 940 nm (LED: 5 mm in diameter; 1.2 V, 50 mA, driven at 5 V using a serial 82 Ohm resistor) were used to illuminate cells while minimizing heat and phototoxicity. The 940 nm wavelength turned out to be an acceptable compromise to avoid phototoxicity and to maintain sufficient resolution power. Plan achromatic objectives (×10: 0.25 NA) (Carl Zeiss Jena, Germany) were used to secure a broad field of view to be imaged. Custom-modified 2 megapixel UVC camera (Asus Computer International, Fremont, CA, USA) boards with USB 2.0 connection served image detection. Cell cultures in glass-bottom dishes were placed under inverse microscopes, and photographs of cells were taken every minute. Ten images were collected, each within the 5-sec interval and averaged to minimize noise. Time-lapse microscopy images were collected every min during a 5-sec pulse of near-infrared -LED illumination and regarded as an optimal time resolution with the possibly lowest phototoxicity [2,3].

2.2.7. Image analysis

During time-lapse microscopy, the National Health Institute's ImageJ software was used to analyze the image sequences (https://fiji.sc). The image analysis method included:

(a) Image restoration and noise reduction: RGB image sequences were converted to an 8-bit grayscale image. Deflickering by using a sequence stack histogram served to avoid transient brightness changes between separated frames. Contrast and brightness were equalized based on the stack (sequence) histogram at 0.4% of the pixels saturated.

Fast Fourier-transformation and background subtraction. The background was reduced by bandpass filtering to exclude large structures down to 40 pixels and filtering small structures up to 3 pixels in size, and background extraction process using a rolling ball at a radius of 50 pixels.

(b) Segmentation: Image sequences were thresholded using a stacked histogram by keeping the information containing elements of the image sequence as foreground, and throwing the redundant pixels away by thresholding them into the background.

(c) Measurement: Thresholding results in a binary image were used for graphical representation.

2.2.8. Size distribution of MWCNT aggregates using time-lapse microscopy images

The determination of the size of aggregated CNTs was based on time-lapse scanning images obtained during cytotoxicity examinations described above. The evaluation of the images was performed employing the ImageJ software program. The Block Matching Parameters (Fiji J) helper plugin was applied for the measurements. Images were converted to the 8-bit formate applying the threshold function. After segmentation, only the aggregates of the binary images remained visible. Segmentation was followed by the analysis of the particles measuring the diameters of particles. Data were obtained in pixels. The microphotographs of the small squares of the Bürker chamber were used for calibration to express pixels in μm-s. The size of CNT aggregates was measured in pixels then converted to μm-s.

The scratch wound assay mimics cell behaviour during wound healing *in vitro* in a confluent cell layer [32]. Control limbal cells in glass-bottom dish were grown in DMEM-F12 + 10% FBS +1% PSN in carbon dioxide incubator at 37°C at 5% CO_2 until confluency (~ 48 h) was attained. After reaching confluency the surface of the monolayer was scratched with a sterile 20 gauge needle and regeneration was traced by time-lapse photomicrography until the disrupted area was healed. White numbers at the bottom of

 doi:10.20944/preprints202304.0986.v1

panels indicate the time of photography in minutes taken from the beginning of time-lapse image analysis.

Time-lapse video microscopy combined with image analysis served to test different parameters including cell growth, reduction of the damaged surface, the regrowth of defect area, motility of cells in the monolayer, the viability of cells [2,28,29]. Limbal cells in the presence of nanotube bundles were grown for the same time as the control population in the carbon dioxide incubator at 37°C at 5% CO_2. When confluency was reached the monolayer was scratched and further grown until the homogeneity of the culture was regained.

2.2.9. Fluorescence microscopy

Limbal stem cell growth mimicking corneal reepithelization, reversible permeabilization of cells, isolation of nuclei, the spread of nuclear structures and fluorescence microscopy have been described [2]. The reason of studying the chromatin condensation patterns was to show that reepithelization process does not generate dead cells seen as large disrupted necrotic cells, or small apoptotic bodies. Briefly, two inverse microscopes, placed in a CO_2 incubator, were equipped with high-sensitivity digital cameras and connected to a dual image-acquisition computer system. Illumination was developed to minimize heat- and phototoxicity. Operation of the spectrally cold-white light emitting diodes was synchronized with image-acquisition periods. Frames were recorded every minute and the whole video sequence was converted to database form. The time of exposure was indicated in the right lower corner of each frame. Exposures were converted to video films by speeding up the projection to 30 exposures/seconds. The Carl Zeiss Photomicroscope II was used, with UV illuminating light produced by the XBO (150 W/1) vapour lamp.

2.2.10. Cell attachment, division and reattachment

Cells growth and division of individual HaCaT cells served as an example to explain the attachmemt and reattachment of dividing cell during TLM. Close to the tme of cell division healthy cells rounded up and detached from the monolayer. Cell division lastted for about 10 min. After detachment the cell rounding (20 min) was followed by the division and the appearance oftwo round daughter cells (30 min), their gradual separation (40-50 min), the attachment to the surface of the T-flask (60 min) [33].

2.2.11. Chromatin changes during cell death

Generally known chromatin changes follow cellular distortions including rounding up of cells, detachment from the monolayer in cell cultures, blebbing, shrinkage, undergoing a so called apoptotic dance causing apoptosis or swelling and disruption of cells characteristic to necrosis [34].

2.2.12. In vivo murine scratch model mimicking corneal reepithelization

Eight mice (4 males, 4 females) were anaesthetized with 50 mg/kg sodium pentobarbital *i.p.* and the cornea of one of their eyes was scratched with a 32 Gauge hypodermic needle. The first control group (2 mice) did not get any treatment only 2x10 µl saline was dropped into the eye. The eyes of the second control (2 animals) were scratched and saline eye drops were given that did not contain MWCNT. The eyes of the third group (4 mice) were scratched and the scratches were immediately treated with 2 x 10 µl eye drops of saline containing 500 µg/ml MWCNT. Mice were kept under regular breeding conditions. Photographs of the eyes were taken twelwe day as after treatment. In another experiment 12 days after 500 µg/ml, MWCNT treatment mice were euthanized with a 300 mg/kg intravenous injection of sodium pentobarbital. The eyes of this *post mortem* group were removed washed with saline and examined with a stereomicroscope at 20x magnification and photographed.

 doi:10.20944/preprints202304.0986.v1

3. Results

3.1. Size distribution and cytotoxicity of MWCNT aggregates

The cornea is exposed every day to different types of nanomaterial aggregates. To mimic cornea exposure multi-walled carbon nanotubes of 10-30 nm outer diameter and 10-30 μm length were used. The size distribution of MWCNT bundles in PBS varied within a relatively broad spectrum explained by the aggregation of MWCNTs dispersed in cell culture media. The measurement of size distribution given in Fig. 2 shows that aggregates of CNTs are much larger than nanotubes and are in the 30 – 200 μm size range.

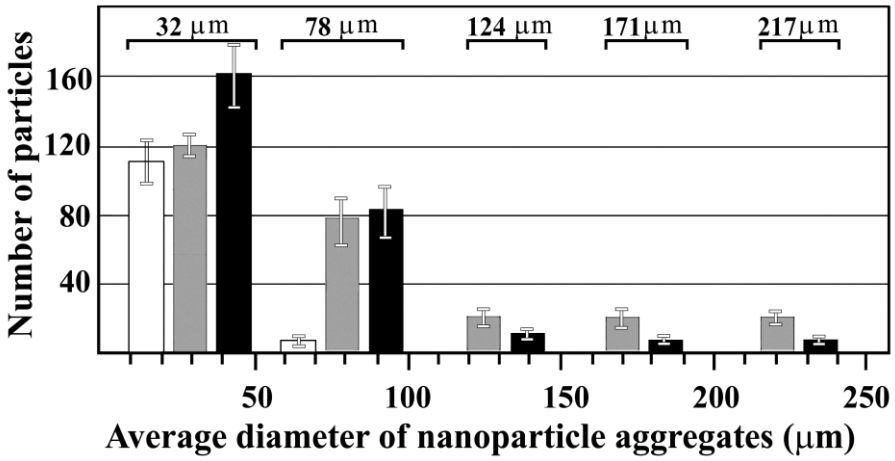

Figure 2. The average diameter of MWCNTs suspended in PBS. Dispersion measurements were performed immediately after suspension, sonication and vortexing. MWCNT concentrations: 5 μg/ml (□),50 μg/ml (▒), 100 μg/ml (■). Aggregation prevented the determination of the size of bundles at 500 μg/ml MWCNT concentration. It is important to note that this work does not deal with dispersed carbon nanotubes but with aggregated MWCNT bundles.

Cytotoxicity detection of CNT bundles was based on the measurement of different parameters including cell growth, regeneration of damaged cells surface, reduction of the damaged surface, motility of cells in the monolayer using time-lapse microscopy and trypan blue dye exclusion viability test at different MWCNT concentrations.

3.2. Growth curves in the absence and presence of MWCNT aggregates

It was expected that MWCNTs could exert a time- and concentration-dependent cytotoxicity on HuLi epithelial cells. HuLi cells were grown for three days in the presence of different concentrations of nanotubes. The monolayer growth curves of HuLi cells in the presence of MWCNT showed some delay in the growth and steepness of the slope shown in Fig. 3A, but no visible signs of apoptosis or necrosis were observed. This figure shows the analysis of the image sequences of the 60 h cytotoxicity measurements of MWCNT aggregates. The monolayer growth of the control is shown in the absence of MWCNT aggregates in the upper panel of Fig. 3A. In the presence of 5 μg/ml MWCNT aggregates the growth was similar to the control and the confluency reached more than 90% in 60 h, indicating that at this concentration the MWCNTs did not exert considerable cytotoxicity. In the presence of 50 μg/ml MWCNT aggregates the growth was linear up to 60 h with a maximal 90% monolayer growth. After reaching an 80% plateau in about 42 h there was no further growth in the presence of higher (100 μg/ml) MWCNTs concentration, indicating the prevention of growth rather than the toxicity of nanotube aggregates. In the presence of 500 μg/ml, MWCNTs concentration macroaggregate formation was so dense that it obscured the picture (not shown).

Preprints (www.preprints.org) | NOT PEER-REVIEWED | Posted: 26 April 2023 doi:10.20944/preprints202304.0986.v1

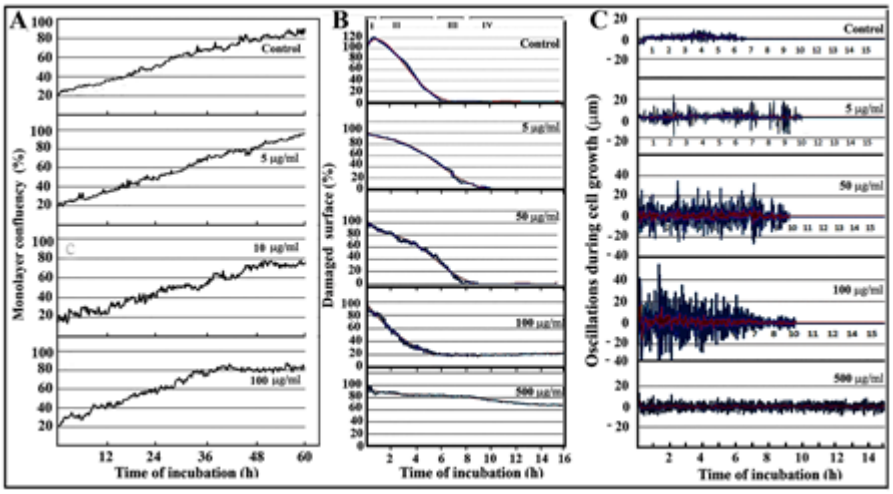

Figure 3. Cytotoxicity of MWCNTs. A) The growth of four HuLi cell cultures was started at 20% confluency and grown for 60 h in the absence, in the presence of 5 μg/ml, 50 μg/ml, and 100 μg/ml MWCNT, respectively. Increasing confluencies are given in percentages. B) Regeneration of damaged limbal cell monolayer in the absence (control) and the presence of 5, 50, 100, and 500 μg/ml MWCNT. Distinguishable phases in the profile of the control curve are indicated by *i, ii, iii* and *iv.* C) Motility of limbal cells in the absence and presence of MWCNTs. Lowest motility during the regeneration of scratched surface in the absence of MWCNTs. Increased motility in the presence of MWCNT as a function of nanoparticle concentration (5-100 μg/ml). Resistance against monolayer regeneration at high (500 μg/ml) MWCNT.

As far as the distinguishable subphases in the regeneration process of control and at low (5 μg/ml) concentration of MWCNTs treated are concerned, in the presence of higher concentration (50 μg/ml) of nanotubes the following observations were made. *i).* The formation of the edges of the scratched surface lasted longer (~ 1 h). *ii)* Reattachment of the damaged monolayer in the presence of nanotube aggregates lasted longer for ~ 1 h. *iii)* The increase in cell growth was less steep taking about 3 h. *iv)* The transition to confluency took more time (2 h 20 min) than in the control population. At higher (100, 500 μg/ml) MWCNTs concentration the borders of subphases disappeared. The most characteristic changes were seen when the mobility changes of HuLi cells were measured.

3.3. Motility changes in the scratched monolayer

The monolayer of the control population that was not subjected to MWCNTs treatment was grown to 100% confluency, then damaged by scratching the surface and regeneration was followed by time-lapse microscopy (Fig. 3B). Motility fluctuations in the control population oscillated in a narrow range allowing fast reattachment and regeneration of the scratched surface. Motility changes in the control population (Fig. 3C, upper panel) were measured up to the end of the regrowth of the monolayer (210 min), followed by a gradually declining motility of cells between 210 and 330 min. Finally, cells were confined to baseline motion after the monolayer reached confluency. Similarly to the regeneration curve, the visual images of time-lapse microscopy showed that the regeneration of the torn apart monolayer surface to complete confluency in healthy untreated cells took about 320 min.

Results presented in Fig. 3C indicate that the fast regeneration of the control population is due to the existing adherent mesh between the scratched monolayer and the growth surface. The regeneration is slowed down in a concentration-dependent manner by the presence of MWCN aggregates (5-100 μg/ml) as indicated by the increasing oscillations in the motility and lagging growth. At the highest concentration of MWCNTs (500 μg/ml) nanoparticle aggregation prevented the motion of cells and terminated the regeneration process.

Preprints (www.preprints.org) | NOT PEER-REVIEWED | Posted: 26 April 2023 doi:10.20944/preprints202304.0986.v1

3.4. Time-lapse microscopy of regenerating limbal cell monolayer

The healing of the damaged monolayer in the absence of MWCNT aggregates is demonstrated by our reepithelization sensing system based on time-lapse microscopy. The visual images of time-lapse microscopy showed that the regeneration of the torn apart monolayer surface to complete wound healing in untreated cells took about 320 min (Fig. 4a) (Video 1).

In the presence of 5 μg/ml MWCNT, few aggregates are seen as black dots (Fig. 4b) (Video 2), the regeneration process lasted for about 530 min. Time-lapse photomicrography showed how the scratched monolayer surface disappeared during the regeneration until the disrupted area was healed. Large black dots indicated the presence of clamped together nanoparticle aggregates at 50 μg/ml concentration.

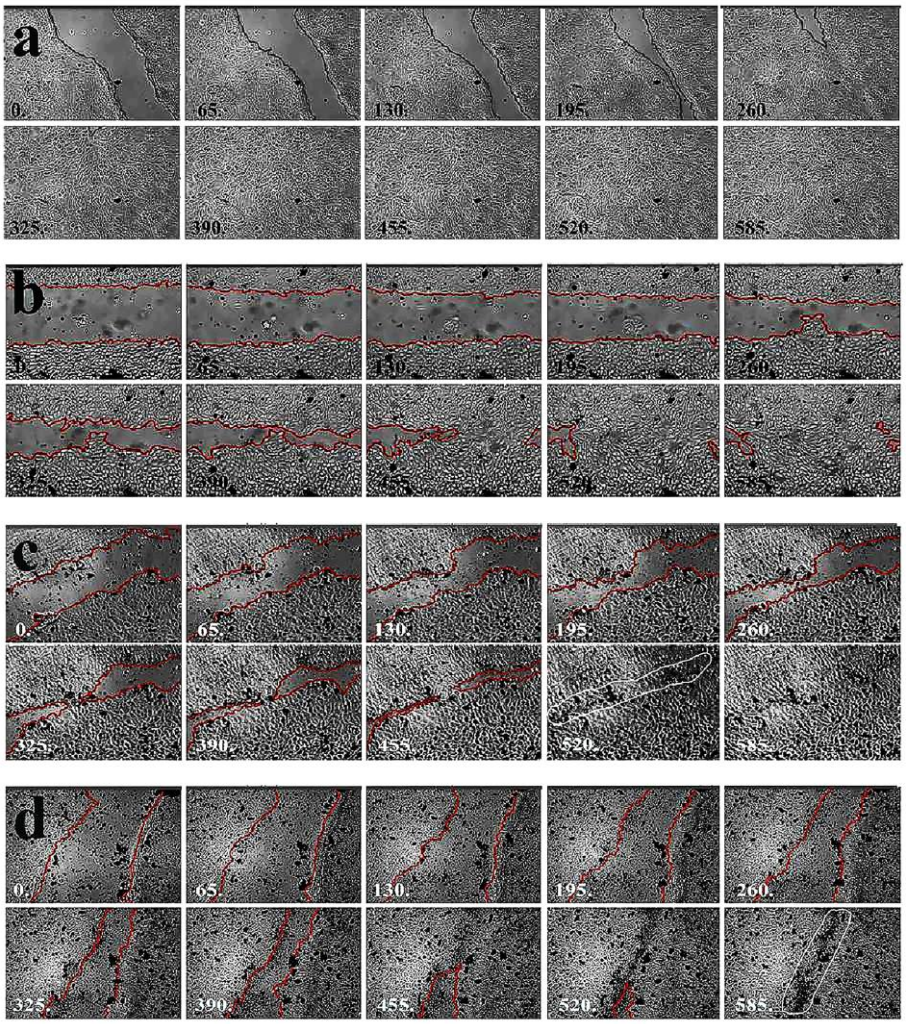

Figure 4. Regeneration of damaged limbal cell monolayer in the absence of nanoparticles followed by time-lapse microscopy. After reaching confluency the surface of the monolayer was scratched with a sterile 20 gauge needle and regeneration was traced by time-lapse photomicrography until the disrupted area was healed. White numbers at the bottom of panels indicate the time of photography in minutes taken from the beginning of time-lapse image analysis. Scar formation is indicated by the surrounded area.

Scar formation seen as a black dotted curve in the confluent monolayer indicated that the closing monolayer squeezed the macroaggregates in front of the narrowing edges of the scratch. Although, nearly complete confluency could be reached at 50 μg/ml or higher nanotube concentration (Fig. 4c) (Video 3), due to the scar formation (white circled area) of macroaggregates such contamination would not be tolerable in ophthalmology.

Preprints (www.preprints.org) | NOT PEER-REVIEWED | Posted: 26 April 2023 doi:10.20944/preprints202304.0986.v1

At 100 μg/ml, MWCNTs (Fig. 4d) (Video 4) concentrations scar formation (white circled areas) was more pronounced, but regeneration was completed after about 530 min corresponding to the regrowth observed in the presence of 50 μg/ml MWCNTs. These observations suggest that nanotubes do not influence cell growth, but their presence causes the formation of macroaggregates that are trapped between the narrowing edges of the scratch generating a black scar, which would seriously interfere with the proper eyesight of patients.

In the presence of 500 μg/ml, MWCNTs cell growth was inhibited and did not go further than 45% in 12 h. The cell motility was reduced and the closure of the narrowing scratch was prevented by the macroaggregates embedded in the monolayer, forming large black bands. The size of macroaggregates could not be measured in the monolayer as the narrowing gap compressed the particles (Video 5).

3.5. Spread of monolayer in regions of interest

For the full field of view analysis, regions of interests were selected randomly all over the edge of scratches (n=5). The reattachment and migration of dividing cells were expressed by a joint term representing the spread in selected regions of interest (ROIs). The averages of negative (cell death, shrinkage, transient detachment of dividing cells) and positive (reattachment, cell division) movements characteristic to individual concentrations of MWCNTs of 300 x 150 μm ROIs are summarized in Table 1.

Table 1. Spread of monolayer in the presence of different concentrations of MWCNT. Table 5. μg/ml MWCNT is given in μm^2/min measured at the edges of 5.

Monolayer spread (μm^2/min)		MWCNT (μg/ml)			
	Control	5	50	100	500
in ROIs	62.94 ± 8.2	41.21 ± 6.3	40.12 ± 4.4	38.90 ± 4.1	n.m.

Selected regions of scratches; n.m. – not-measurable.

MWCNTs slow down the spread of the monolayer (Table 1). It deserves to mention that the reduction of the speed of the monolayer spread (~40 μm^2/min) in the selected regions and at the edges of the scratches did not differ significantly within the 5-100 μg/ml concentration range of MWCNTs. Corresponding to the reduced speed of growth, the time of was uniformly extended from the control 320 min to 530 min in MWCNTs treated monolayers. At a high (500 μg/ml) concentration of MWCNTs, the regeneration of the monolayer was incomplete due to the large nanotube aggregates that prevented the motility of limbal cells. Consequently, motility values at (500 μg/ml) concentration of MWCNTs were low.

3.6. Viability of MWCNT treated cells

The viability of HuLi stem cells was counted in the Bürker chamber after 18 h of MWCNTs treatment using the trypan blue dye exclusion test. Fig. 5 shows some tendency of losing viable cells upon the presence of MWCNT aggregates. However, the loss of viable cells after treatment presented as mean relative to the initial cell number was not statistically significant. The modest (8.4 %) loss of viability between the 5 μg/ml and 500 μg/ml as well as a merely 1.6 % difference in viability between the 100 and 500 μg/ml MWCNTs treated cell is an indication that it is not primarily the presence of MWCNTs that is accounted for by the moderately reduced viability of HuLi cells.

Preprints (www.preprints.org) | NOT PEER-REVIEWED | Posted: 26 April 2023 doi:10.20944/preprints202304.0986.v1

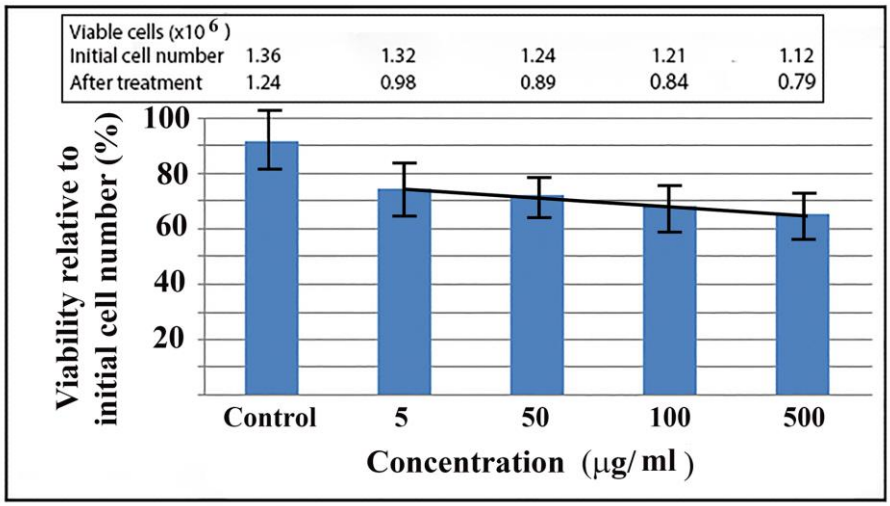

Figure 5. Viability of HuLi cells in the presence of MWCNT. Cells were grown in the presence of different concentrations of nanoparticles for 18 h then subjected to trypan blue staining. Viable cells were expressed in percentages of initial cell numbers.

3.7. Chromatin condensation in the presence of MWCNT aggregates

The common pathway of chromatin condensation in mammalian cells [35] is contrasted by morphological changes, among them chromatin condensation as the most recognizable nuclear hallmark of apoptosis [34]. Apoptotic chromatin changes reflect the type of genotoxic agents by using different apoptotic agents, among them heavy metals (Cd, Pb, Cr, Ni, Ag) and irradiations (alpha, gamma, UV). It turned out that chr4 of characteristic morphological changes such as apoptosis and necrosis than other cellular assays. Indeed chromatin changes are sensitive indicators of genotoxicity at submicromolar and micromolar concentrations [34,35]. Intermediates of chromatin condensation in control stem cells (Fig. 6A, upper left panels) were similar to those seen earlier [16] in limbal cells and other mammalian cells including decondensed chromatin veil, chromatin ribbon, chromatin bodies (early visible forms of chromosomes), elongated early chromosomes and metaphase chromosomes [35]. Despite the increasing MWCNTs concentration, not only prophase but also metaphase chromosomes were observed after each treatment without the formation of apoptotic bodies or necrotic enlarged nuclei.

Preprints (www.preprints.org) | NOT PEER-REVIEWED | Posted: 26 April 2023 doi:10.20944/preprints202304.0986.v1

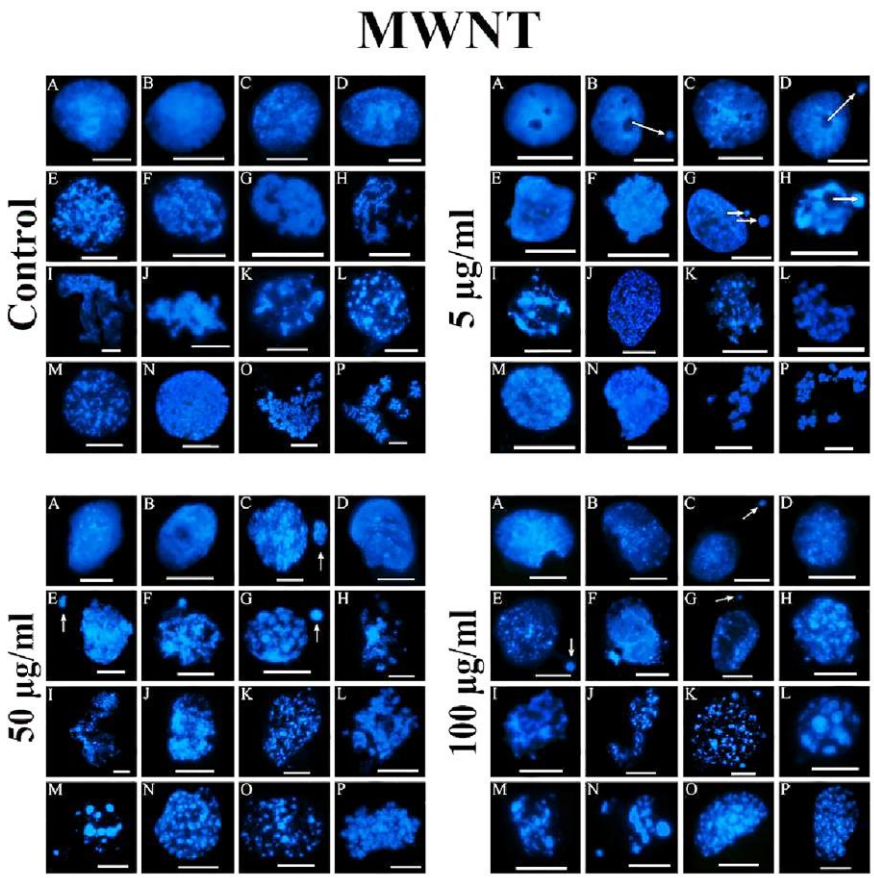

Figure 6. Chromatin condensation in nuclei of limbal cells grown in the absence and the presence of MWNT. A) Control limbal cells were grown in T-25 flasks in DMEM-F12 +10% FBS + 1% PSN in carbon dioxide incubator at 37°C at 5% CO_2, in the absence of nanotubes for 24 h, harvested, reversibly permeabilized and subjected to isolation of nuclei, isolation and visualization of chromatin structures as described earlier (left upper panels). Limbal cells were grown for 24 h in the presence of 5 µg/ml MWCNT, chromatin structures were isolated and visualized the same way (upper right panels). The growth of limbal cells in the presence of 50 µg/ml MWCNT, followed by isolation and visualization of chromatin structures (lower left panels). Limbal chromatin structures after treatment of cells with 100 µg/ml MWCNT (lower right panels). White arrows indicate the presence of micronuclei. Types of chromatin condensation intermediates: A-D, early decondensed chromatin; E-H, chromatin ribbon; F-L, chromatin bodies, the first recognizable chromosomes; M-P, the formation of metaphase chromosomes. Bars, 5 µm each.

Chromatin structures isolated from limbal cells upon subjection to different 5, 50 and 100 µg/ml concentrations of MWCNTs did not show significant differences from those chromatin forms that were isolated from the control population (upper right and lower panels of Fig. 6). One noticeable difference was the appearance of micronuclei (indicated by white arrows) in MWCNTs treated cells and some delay in the pattern of chromatin condensation seen as incomplete condensation of metaphase chromosomes. As chromatin structures are sensitive indicators of cellular toxicity, the lack of chromatin distortions clearly showed that MWCNTs did not exert cytotoxicity on HuLi stem cells. One would expect, if micronuclei are produced, there is DNA damage, therefore there is also cell damage. Micronuclei are regular structures of interphase chromatin condensation. Micronuclei occur not only when cells are damaged and used as an apoptotic testbut regular intermediates of interphase chromatin condensation [36].

3.8. In vivo eye reepithelization in the presence of MWCNT bundles

 doi:10.20944/preprints202304.0986.v1

Control mice were given saline (2x10 µl) dropped into their eyes and photographs were taken (Fig. 7a, b). In the second control group of mice, the scratch was performed on the epithelial surface of the eyes and 2x10 µl saline was dropped into their eyes. Complete eye healing was observed after 12 days (Fig. 7c, d). After dropping low MWCNTs concentration (5 µg/ml) into the scratched eyes complete reepithelization without scar formation or eye irritation were observed. To compensate the removal of MWCNTs from the eyes by blinking and lachrymation the regeneration process of damaged eyes was tested at the highest 500 µg/ml concentration where MWCNTs containing saline was dropped into the scratched surface of the eyes. The healing of the cornea was prevented by macroaggregate formation (Fig. 7 e-h). The size of the macroaggregates in the damaged eyes of mice varied as a consequence of the partial removal of macroaggregates by lachrymation and blinking. Cornea reepithelization was also tested 12 days after reepithelization in the presence of 500 µg/ml MWCNTs with the noticeable difference that animals were euthanized and their eyes were photographed *post mortem* (Fig. 7 i-p) to get a better view than in living animals.

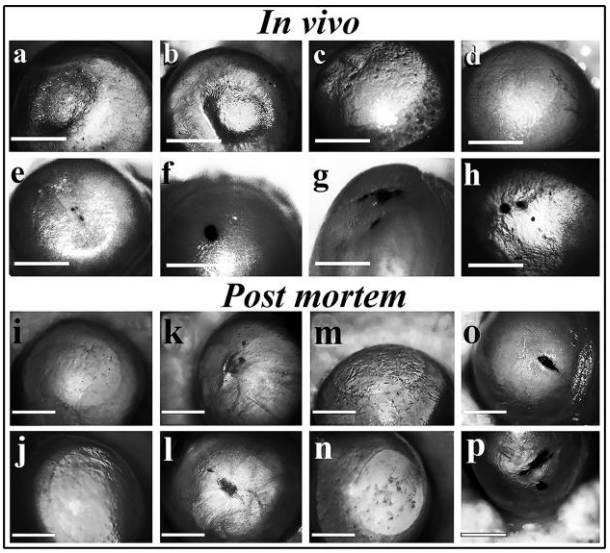

Figure 7. Corneal reepithelization of damaged murine eyes in the absence and presence of MWCNT. Animal experiments were carried out to confirm or deny the toxicity of MWCNTs described in the Experimental Section. *In vivo* experiment: a, b) Control: dropping saline into the eyes of mice without any treatment. c, d) Reepithelization of scratched eyes in the absence of 500 µg/ml MWCNT particles. e-h) Prevention of reepithelization in the presence of 500 µg/ml MWCNT. *Post mortem* experiment: A similar experiment was carried but mice were euthanized, their eyes removed and washed with saline before photography. Control: saline drops alone (i, j), *in vivo* scratch and saline drops without regeneration and immediate photography (k, l), *in vivo* scratch, saline drops and regeneration (m, n), *in vivo* scratch and treatment with saline containing 500 µg/ml MWCNT (o, p). All photographs were taken 12 days after treatment except for k and l.

4. Discussion

Low concentrations of airborne nanotubes and their aggregates have not been tested for their ophthalmological impact although, they belong to daily damages. The release of huge amounts of airborne particles generated in fires, explosions, car exhaust pipes as well as their aggregation could cause scar formation and incomplete regeneration of the damaged cornea. Whereas fullerene soot containing single-walled carbon nanotubes (SWCNTs) caused no visible of health hazard [37], others have observed the cytotoxicity of SWCNTs and apoptosis [38], raising the question whether SWCNTs or MWCNTs exert higher cytotoxicity. It also needs to be explained why others found MWCNTs to interfere with cellular functions whereas in our study MWCNT macroaggregates caused no visible cell death.

Single–walled carbon nanotubes (CWNTs) due to their smaller size, large surface area and high reactivity permeate cellular membranes and attach to biological molecules, inhibit cell growth, induce DNA breakage and generate reactive oxygen species [39]. The cytotoxicity of MWCNTs concerning functionalization suggested that pristine MWCNTs induced cell death but paradoxically functionalized MWCNTs were more genotoxic compared to their pristine form [40]. In contrast, pristine CNTs were more toxic than oxidized CNTs [41] Similarly, to our observations Coccini et al. [42] have observed that the viability of astrocytoma and pneumocyte cells was unaffected by pristine and by functionalized MWCNTs up to 200 μg/ml of these nanotubes in samples incubated for 24 or 48 h.

When the clastogenic/genotoxic potential of functionalized and non-functionalized MWCNTs was investigated in murine bone marrow cells non-functional MWCNTs were toxic only at sufficiently high concentration, whereas functionalized MWCNTs had a higher clastogenic/genotoxic potential than the non-functionalized form of MWCNT [43]. It was concluded that the lower cytotoxicity of MWCNTs than those of SWCNTs could make MWCNTs more suitable for medical applications [44]. The picture that emerged from different functionalizations suggested that the toxicity of MWCNTs is related to their hydrophobicity [45] in agreement with the view that polar pristine MWCNTs do not interact with giant unilamellar vesicles of cells, remain outside the cells and have little or no effect on the viability of these cells [36]. Similarly, multi-walled carbon nanotube oxidation dependent keratinocyte cytotoxicity and skin inflammation were found by Palmer et al. [10]. Similarly, it was found that HaCaT keratinocytes displayed increased cytotoxicity when exposed to MWCNTs with high levels of carboxylation [10].

Interphase chromatin alterations are sensitive indicators of cytotoxicity at submicromolar and micromolar concentrations. The characteristic deformations and shrinkage of nuclei showed a close correlation between the frequency of micronucleus formation and the concentration of the genotoxic agent [46]. Apoptotic agents are known to affect chromatin morphology in a genotoxicity specific manner [46]. In general, nanomaterial cytotoxicity is composition-, size-, cell type- [47] and time-dependent [48]. As far as the cytotoxicity of MWCNTs is concerned, we have observed the reduced number of metaphase chromosomes beside initiating micronucleus formation but they did not cause significant cell death. Increased number of micronuclei was readily detectable in rapidly dividing interphase cells which may also result from clastogenic or aneugenic mechanisms. Micronucleus test is an umbrella term for many differing micronucleus tests [36].

In vivo experiments by scratching the cornea of mice with a hypodermic needle (gauge 20) known as the scratch model and allowing reepithelization in the presence of MWCNTs particles confirmed *in vitro* results. More importantly, the *in vivo* test validated the applicability of time-lapse microscopy that was mimicking faithfully limbal cell regrowth under *in vitro* conditions.

5. Conclusions

Three types of ophthalmological experiments were carried out.

(*i*) In our first study we have mimicked ocular injuries *in vitro* and have followed the regeneration of human limbal cells. time-lapse microscopy was in ophthalmology. During corneal damages, the healing process is regularly prevented by treating damaged eyes with antibiotics (chloramphenicol, rifampicin). We found that antibiotics delayed the *in vitro* regeneration of human limbal cells [2].

(ii) The healing of unprotected damaged eyes in the presence of nanoparticles may extend the healing and is prone to ocular infection. We have selected those nanoparticles that are known for their mild antiseptic (oligodynamic) effect (silver and gold). Our results showed that limbal cell regeneration and chromatin toxicity were dose dependent. In spite of their lower size, Ag nanoparticles (10 nm) were less toxic than larger gold particles (100 nm) [49].

(iii) The third aspect was dealing with gadolinium induced effect on the motility, adherence, and chromatin structure on mammalian cells including HuLi cells. Gadolinium complexes, endocytosed by macrophages and distributed to nuclei, cause apoptosis of macrophages preventing the regeneration of corneal damages [50].

(iv) This paper is dealing with the regeneration of the damaged cornea in the presence of multi-walled carbon nanoparicles. The effect of nanotubes (10-30 μm in length and 10-30 nm in diameter) tested on limbal cell monolayer regeneration, corresponded to the observations of others on different cell lines that MWCNTs did not cause significant toxicity. The explanation to these observations could be that pristine MWCNTs díd do not interact with giant unilamellar vesicles of cells, remain outside the cells and have little or no effect on the viability of these cells [51].

Eyes are exposed every day to low concentrations of airborne nanoparticles, among them nanotubes without notable ophthalmological consequences. However, the increased number of airborne particles upon accidents may cause corneal damages, incomplete regeneration and scar formation. Results confirmed that human limbal cell regrowth upon corneal trauma mimicked by the *in vitro* scratch model was slowed down. Low concentrations of nanomaterials including MWCNTs caused neither significant corneal irritation, nor cell death, nor pulmonary damages in rodents [47].

Nevertheless, high concentrations of MWCNTs are prone to form aggregates in corneal wounds. These deposits have to be removed or at least minimized before other ophthalmic treatments. These observations are of medical importance and suggest that when the cornea is exposed to the sudden release of high concentrations of nanoparticles, due to their strong absorption they cannot be removed with ophthalmic fluids. Special coating for the removal of aggregated nanotubes with adherent materials deserves further investigation. Finally, *in vivo* results confirmed the validity of *in vitro* tests and suggested that time-lapse microscopy could be a useful model to follow the regeneration of cellular damages.

Author's contributions: Conceptualization: G.S-N., G.B., V.B., A.K.; Collection and assembly of data: V.B., M.T., A.K., Z.M. S.; G.S-N.;G.P. Data analysis and interpretations: G.B., G. S-N., V. B., M.T.; Manuscript writing: G.B., G. S-N., M.T.; Approval of the manuscript: All authors; Accountable for all aspects of the work: G.B., G. S-N.

Funding: This work was supported by TÁMOP 4.2.4. to G. S-N and by the HungarianNational Science and Research Foundation OTKA 42762 grant to G.B.

Institutional ReviewBoard Statement: Not relevant to this study.

Informed Availability Statement: Not applicable.

Conflicts of Interest: The authors declare to have no competing interests. This includes the founder-related design of the study; in the collection, analyses, or in the terpretation of data; in the writing of the manuscript; or in the decision to publish the results.

Ethics approval and consent to participate: Animal and human care were secured in our Experimental Animal care facility (reg. number III/3-KÁT/2015) under the supervision of Animal Care Committee, University of Debrecen (licence number 2/2014 DEMAB).

Consent for publication: All authors gave their consent to publish before the submission of the work to Int. J. Mol. Sci

Availability of data and materia: The authors confirm that the data supporting the findings of this study are available within the article. Supplementary material associated with this article can be found at https://...

Acknowledgments: The technical assistance of Miss P. Keresztesi is gratefully acknowledged.

References

1. Liang, C.C.; Park, A.Y.; Guan, J.L. In vitro scratch assay: a convenient and inexpensive method for analysis of cell migration in vitro. Nat. Protoc. 2007, 2(2), 329-333. doi:10.1038/nprot.2007.30.

2. Turani, M.; Banfalvi, G.; Peter, A.; Kukoricza, K.; Kiraly, G.; Talas, L.; Tanczos, B.; Dezso, B.; Nagy, G.; Kemeny-Beke, A. Antibiotics delay in vitro human stem cell regrowth. Toxicol. In Vitro 2015, 29(2), 370-379. doi:10.1016/j.tiv.2014.10.013.
3. Turani, M.; Banfalvi, G.; Kukoricza, K.; Jakim, J.; Pocsi, I.; Kemeny-Beke, A.; Nagy, G. Regeneration of limbal stem cells in the presence of silver and gold nanoparticles. J. Environ. Anal. Toxicol. 2015, 5:5. 318. doi:10.4172/2161-0525.1000318.4. Fröhlich, E.; Meindl, C.; Höfler, A.; Leitinger, G.; Roblegg, E. Combination of small size and carboxyl functionalisation causes cytotoxicity of short carbon nanotubes. Nanotoxicology 2013, 7(7), 1211-1224. doi:10.3109/17435390.2012.729274.
5. Simon-Deckers, A.; Gouget, B.; Mayne-L'hermite, M.; Herlin-Boime, N.; Reynaud, C.; Carrière, M. In vitro investigation of oxide nanoparticle and carbon nanotube toxicity and intracellular accumulation in A549 human pneumocytes. Toxicology 2008, 253(1-3), 137-146. doi:10.1016/j.tox.2008.09.007.
6. Assali, M.; Zaid, A.N.; Kittana, N.; Hamad, D.; Amer, J. Covalent functionalization of SWCNT with combretastatin A4 for cancer therapy. Nanotechnology 2018, 29(24), 245101. doi:10.1088/1361-6528/aab9f2.
7. Ding, Y.; Tian, R.; Yang, Z.; Chen, J.; Lu, N. Effects of serum albumin on the degradation and cytotoxicity of single-walled carbon nanotubes. Biophys. Chem. 2017, 222, 1-6. doi:10.1016/j.bpc.2016.12.002.
8. Maruyama, K.; Haniu, H.; Saito, N.; Matsuda, Y.; Tsukahara, T.; Kobayashi, S.; Tanaka, M.; Aoki, K.; Takanashi, S.; Okamoto, M., et al. Endocytosis of Multiwalled Carbon Nanotubes in Bronchial Epithelial and Mesothelial Cells. Biomed. Res. Int. 2015, 2015. 793186, doi:10.1155/2015/793186.
9. Requardt, H.; Braun, A.; Steinberg, P.; Hampel, S.; Hansen, T. Surface defects reduce Carbon Nanotube toxicity in vitro. Toxicol. In Vitro. 2019, 60, 12-18. doi:10.1016/j.tiv.2019.03.028.
10. Palmer, B.C.; Phelan-Dickenson, S.J.; DeLouise, L.A. Multi-walled carbon nanotube oxidation dependent keratinocyte cytotoxicity and skin inflammation. Part. Fibre Toxicol. 2019, 16(1), 3. doi:10.1186/s12989-018-0[5-x.
11. Guo, B.; Liao, C.; Liu, X.; Yi, J. Preliminary study on conjugation of formononetin with multiwalled carbon nanotubes for inducing apoptosis via ROS production in HeLa cells. Drug Des Devel. Ther. 2018, 12, 2815-2826. doi:10.2147/dddt.S169767.
12. Snyder-Talkington, B.N.; Dong, C.; Singh, S.; Raese, R.; Qian, Y.; Porter, D.W.; Wolfarth, M.G.; Guo, N.L. Multi-Walled Carbon Nanotube-Induced Gene Expression Biomarkers for Medical and Occupational Surveillance. Int. J. Mol. Sci. 2019, 20(18), 4431. doi:10.3390/ijms20112635.
13. Pacurari, M.; May, I.; Tchounwou, P.B. Effects of lipopolysaccharide, multiwalled carbon nantoubes, and the combination on lung alveolar epithelial cells. Environ. Toxicol. 2017, 32(2), 445-455. doi:10.1002/tox.22248.

14. Emerce, E.; Ghosh, M.; Öner, D.; Duca, R.C.; Vanoirbeek, J.; Bekaert, B.; Hoet, P.H.M.; Godderis, L. Carbon Nanotube- and Asbestos-Induced DNA and RNA Methylation Changes in Bronchial Epithelial Cells. Chem. Res. Toxicol. 2019, 32(5), 850-860. doi:10.1021/acs.chemrestox.8b00406.
15. Ma-Hock, L.; Treumann, S.; Strauss, V.; Brill, S.; Luizi, F.; Mertler, M.; Wiench, K.; Gamer, A.O.; van Ravenzwaay, B.; Landsiedel, R. Inhalation toxicity of multiwall carbon nanotubes in rats exposed for 3 months. Toxicol. Sci. 2009, 112(2), 468-481. doi:10.1093/toxsci/kfp146.
16. Liu, Y.; Zhao, Y.; Sun, B.; Chen, C. Understanding the toxicity of carbon nanotubes. Acc. Chem. Res. 2013, 46(3), 702-713. doi:10.1021/ar300028m.
17. Madani, S.Y.; Mandel, A.; Seifalian, A.M. A concise review of carbon nanotube's toxicology. Nano. Rev. 2013, 4(1). doi:10.3402/nano.v4i0.21521.
18. Allegri, M.; Perivoliotis, D.K.; Bianchi, M.G.; Chiu, M.; Pagliaro, A.; Koklioti, M.A.; Trompeta, A.A.; Bergamaschi, E.; Bussolati, O.; Charitidis, C.A. Toxicity determinants of multi-walled carbon nanotubes: The relationship between functionalization and agglomeration. Toxicol. Rep. 2016, 3, 230-243. doi:10.1016/j.toxrep.2016.01.011.
19. Uibel, S.; Takemura, M.; Mueller, D.; Quarcoo, D.; Klingelhoefer, D.; Groneberg, D.A. Nanoparticles and cars - analysis of potential sources. J. Occup. Med. Toxicol. 2012, 7(1), 13. doi:10.1186/1745-6673-7-13.
20. Nomura, M.; Shanmuga Ramanan, S.M.; Arun, S. Automobile Bumpers. In Comprehensive Composite Materials II, Beaumont, P.W.R., Zweben, C.H., Eds. Elsevier: Oxford, 2018; 10.1016/B978-0-12-803581-8.03962-Xpp. 460-468. ISBN 978-0-08-100534-7.
21. Armstrong, G.W.; Chen, A.J.; Linakis, J.G.; Mello, M.J.; Greenberg, P.B. Motor vehicle crash-associated eye injuries presenting to U.S. emergency departments. West. J. Emerg. Med. 2014, 15(6), 693-700. doi:10.5811/westjem.2014.5.20623.
22. Chaurasia, S.S.; Lim, R.R.; Lakshminarayanan, R.; Mohan, R.R. Nanomedicine approaches for corneal diseases. J. Funct. Biomater. 2015, 6(2), 277-298. doi:10.3390/jfb6020277.
23. Osei-Bempong, C.; Figueiredo, F C.; Lako, M. The limbal epithelium of the eye - A review of limbal stem cell biology, disease and treatment. Bioassays, 2013, 35, 211-219
24. Ahmad, S. Concise review: limbal stem cell deficiency, dysfunction, and distress. Stem Cells Transl Med. 2012,

1, 110–115, doi: 10.5966/ sctm.2011-0037
25. Dziasko, M. A.; Daniels, J. T. Anatomical Features and Cell-cell interactions in the human limbal epithelial stem cell niche. Ocular Surface. 2016, 14, 322-330
26. Nuzzi, R.; Buono, L.; Scalabrin, S.; De Iuliis, M.; Bussolati, B. Effect of stem cell-derived extracellular vesicles on damaged human corneal endothelial cells. Stem Cells Internat. 2021 | Article ID 6644463
27. Kang, B.; Chang, S.; Dai, Y.; Yu, D.; Chen, D. Cell response to carbon nanotubes: size-dependent intracellular uptake mechanism and subcellular fate. Small 2010, 6(21), 2362-2366. doi:10.1002/smll.201001260.
28. Huczko, A.; Lange, H. Carbon Nanotubes: Experimental Evidence for a Null Risk of Skin Irritation and Allergy. Fullerene Sci. Techn. 2001, 9(2), 247-250. doi:10.1081/FST-100102972.
29. Albert, R.; Vereb, Z.; Csomos, K.; Moe, M.C.; Johnsen, E.O.; Olstad, O.K.; Nicolaissen, B.; Rajnavolgyi, E.; Fesus, L.; Berta, A., et al. Cultivation and characterization of cornea limbal epithelial stem cells on lens capsule in animal material-free medium. PLoS One 2012, 7(10), e47187. doi:10.1371/journal.pone.0047187.
30. Nagy, G.; Hennig, G.W.; Petrenyi, K.; Kovacs, L.; Pocsi, I.; Dombradi, V.; Banfalvi, G. Time-lapse video microscopy and image analysis of adherence and growth patterns of Candida albicans strains. Appl. Microbiol. Biotechnol. 2014, 98(11), 5185-5194. doi:10.1007/s00253-014-5696-5.
31. Liu, A.; Sun, K.; Yang, J.; Zhao, D. Toxicological effects of multi-wall carbon nanotubes in rats. J. Nanopart. Res. 2008, 10(8), 1303-1307. doi:10.1007/s11051-008-9369-0.
32. Kasper, M.; Moll, R.; Stosiek, P.; Karsten, U. Patterns of cytokeratin and vimentin expression in the human eye. Histochemistry. 1988, 89(4), 369-377. doi:10.1007/bf00500639.
33. Nagy, G.; Pinter, G.; Kohut, G.; Adam, A.L.; Trencsenyi, G.; Hornok, L.; Banfalvi, G. Time-lapse analysis of cell death in mammalian and fungal cells. DNA Cell Biol. 2010, 29(5), 249-259. doi:10.1089/dna.2009.0980.
34. Banfalvi, G. Apoptotic agents inducing genotoxicity-specific chromatin changes. Apoptosis 2014, 19(9), 1301-1316. doi:10.1007/s10495-014-1018-8.
35. Banfalvi, G.; Nagy, G.; Gacsi, M.; Roszer, T.; Basnakian, A.G. Common pathway of chromosome condensation in mammalian cells. DNA Cell Biol. 2006, 25(5), 295-301. doi:10.1089/dna.2006.25.295.
36. Kiraly, G.; Simonyi, A.S.; Turani, M.; Juhasz, I.; Nagy, G.; Banfalvi, G. Micronucleus formation during chromatin condensation and under apoptotic conditions. Apoptosis 2017, 22(2), 207-219. doi:10.1007/s10495-016-1316-4.
37. Aoshima, H.; Saitoh, Y.; Ito, S.; Yamana, S.; Miwa, N. Safety evaluation of highly purified fullerenes (HPFs): based on screening of eye and skin damage. J. Toxicol. Sci. 2009, 34(5), 555-562. doi:10.2131/jts.34.555.
38. Liu, A.; Sun, K.; Yang, J.; Zhao, D. Toxicological effects of multi-wall carbon nanotubes in rats. J. Nanopart. Res. 2008, 10(8), 1303-1307. doi:10.1007/s11051-008-9369-0.
39. Kim, J.S.; Yu, I.J. Single-wall carbon nanotubes (SWCNT) induce cytotoxicity and genotoxicity produced by reactive oxygen species (ROS) generation in phytohemagglutinin (PHA)-stimulated male human peripheral blood lymphocytes. J. Toxicol. Environ. Health A. 2014, 77(19), 1141-1153. doi:10.1080/15287394.2014.917062.
40. Zhou, L.; Forman, H.J.; Ge, Y.; Lunec, J. Multi-walled carbon nanotubes: A cytotoxicity study in relation to functionalization, dose and dispersion. Toxicol. In Vitro 2017, 42, 292-298. doi:10.1016/j.tiv.2017.04.027.
41. Kumarathasan, P.; Breznan, D.; Das, D.; Salam, M.A.; Siddiqui, Y.; MacKinnon-Roy, C.; Guan, J.; de Silva, N.; Simard, B.; Vincent, R. Cytotoxicity of carbon nanotube variants: a comparative in vitro exposure study with A549 epithelial and J774 macrophage cells. Nanotoxicology 2015, 9(2), 148-161. doi:10.3109/17435390.2014.902519.
42. Coccini, T.; Roda, E.; Sarigiannis, D.A.; Mustarelli, P.; Quartarone, E.; Profumo, A.; Manzo, L. Effects of water-soluble functionalized multi-walled carbon nanotubes examined by different cytotoxicity methods in human astrocyte D384 and lung A549 cells. Toxicology 2010, 269(1), 41-53. doi:10.1016/j.tox.2010.01.005.
43. Patlolla, A.K.; Hussain, S.M.; Schlager, J.J.; Patlolla, S.; Tchounwou, P.B. Comparative study of the clastogenicity of functionalized and nonfunctionalized multiwalled carbon nanotubes in bone marrow cells of Swiss-Webster mice. Environ. Toxicol. 2010, 25(6), 608-621. doi:10.1002/tox.20621.
44. Jia, G.; Wang, H.; Yan, L.; Wang, X.; Pei, R.; Yan, T.; Zhao, Y.; Guo, X. Cytotoxicity of carbon nanomaterials: single-wall nanotube, multi-wall nanotube, and fullerene. Environ. Sci. Technol. 2005, 39, 1378-1383. doi:10.1021/es048729l.
45. Pérez-Luna, V.; Cisneros, M.; Bittencourt, C.; Saucedo-Orozco, I.; Quintana, M. Imaging carbon nanostructures' reactivity: a complementary strategy to define chemical structure. R. Soc. Open Sci. 2018, 5(8), 180605. doi:10.1098/rsos.180605.
46. Doherty, A.; Bryce, S.M.; Bemis, J.C. Chapter 6 - The In Vitro Micronucleus Assay. In Genetic Toxicology Testing, Proudlock, R., Ed. Academic Press: Boston, 2016; 10.1016/B978-0-12-800764-8.00006-9pp. 161-205. ISBN 978-0-12-800764-8.
47. Beyeler, S.; Chortarea, S.; Rothen-Rutishauser, B.; Petri-Fink, A.; Wick, P.; Tschanz, S.A.; von Garnier, C.; Blank, F. Acute effects of multi-walled carbon nanotubes on primary bronchial epithelial cells from COPD patients. Nanotoxicology 2018, 12(7), 699-711. doi:10.1080/17435390.2018.1472310.
48. Kolle, S.N.; Sauer, U.G.; Moreno, M.C.; Teubner, W.; Wohlleben, W.; Landsiedel, R. Eye irritation testing of

 doi:10.20944/preprints202304.0986.v1

nanomaterials using the EpiOcular™ eye irritation test and the bovine corneal opacity and permeability assay. Part. Fibre Toxicol. 2016, 13(1), 18. doi:10.1186/s12989-016-0128-6.
49. Banfalvi, G.; Nagy, G. Interphase chromatin structures of human cells. DNA Cell Biol. 2011, 30(12), 1007-1009. doi: 10.1089/dna.2011.1288.
50. Nagy, G.; Baksa, V.; Kiss, A.; Turani, M.; Banfalvi, G. Gadolinium induced effects on mammalian cell motility, adherence and chromatin structure. Apoptosis 2017, 22, 188–199. https://doi.org/10.1007/s10495-016-1311-9.
51. Tan, X.-M.; Lin, C.; Fugetsu, B. Studies on toxicity of multi-walled carbon nanotubes on suspension rice cells. Carbon 2009, 47(15), 3479-3487. doi:10.1016/j.carbon.2009.08.018.